Available online at www.sciencedirect.com
ScienceDirect
Journal of Bionic Engineering 14 (2017) 26–33

Design and Characterization of Magnetically Actuated Helical Swimmers at Submillimeter-scale

Lefeng Wang, Huichao Xu, Wenhe Zhai, Bensong Huang, Weibin Rong

State Key Laboratory of Robotics and System, *Harbin Institute of Technology*, *Harbin* 150080, *China*

Abstract

Bacteria with helical flagella show an ideal mechanism to swim at low Reynolds number. For application of artificial microswimmers, it is desirable to identify effects of structural and geometrical parameters on the swimming performance. In this study, a double-end helical swimmer is proposed based on the usual single-end helical one to improve the forward-backward motion symmetry. The propulsion model of the artificial helical microswimmer is described. Influences of each helix parameter on the swimming velocity and propulsion efficiency are further analyzed. The optimal design for achieving a maximum propulsion velocity of submillimeter scale swimmers is performed based on some constraints. An experimental setup consisting of three-pair of Helmholtz coils is built for the helical microswimmers. Experiments of microswimmers with several groups of parameters were performed, and the results show the validity of the analysis and design.

Keywords: double-end helical microswimmers, magnetic actuation, swimming velocity, optimal design

doi: 10.1016/S1672-6529(16)60375-X

1 Introduction

Microswimmers have numerous potential applications in biomedical engineering and microfluidic systems. In biomedical fields, they can be used for in vivo diagnosis, targeted drug delivery and minimally invasive microsurgery[1–4]. In microfluidic systems, microswimmers can be utilized to manipulate various microobjects for specific tasks[5]. For the power supply of microswimmers, there have been several methods proposed[6–9]. Among them, the use of external magnetic fields has several advantages, such as the magnetic fields are biocompatible at low power levels, the speed and direction of the swimmers are easy to control[10].

For the magnetic actuation, several actuation mechanisms have been used, such as pulling with field gradient[11], swimming with a helical propeller[12,13], swimming with an elastic tail[14,15]. Among these mechanisms, gradient-based pulling is direct but the propulsive force and the maximum speed of the swimmer are small in high-viscosity liquids. Elastic flagellum and rigid helical flagella can produce comparable maximum speed assuming the same cross section and flagella length[16]. Compared to the flexible flagella, the rigid helical flagella is easy to change the motion direction by changing the direction of the rotating magnetic field. Swimmers with helical propellers have been proven to be effective in low-Reynolds-number conditions. Much work has been done on the helical swimmers. Zhang *et al*. developed an artificial bacteria flagella with dimensions of several micrometers. It consists of a helical tail and a soft magnetic head[17]. Xu *et al*. investigated scaled-up helical swimmers with dimensions of several millimeters[18]. The rotational propulsion characteristics of several helical swimmers with different head shapes and tail dimensions were clarified. However, effects of structural and geometrical parameters on motion performances at sub-millimeter scale have not been studied in detail, and the optimal design of the helical parameters have to be explored for future applications.

Due to the manufacturing and measurement limits, it is difficult to characterize the performances of swimmers with only several micrometer size systematically. Although centimeter or millimeter swimmers are easy to be fabricated or characterized, the effect of

Corresponding author: Lefeng Wang
E-mail: lefengwang@hit.edu.cn

gravitation may bring some differences with real microswimmers. In this paper, we focus on the design and characterization of submillimeter-scale swimmers.

This paper is organized as follows. Section **2** describes structures of two artificial microswimmers. Section **3** models the helical swimmer, and the swimming velocity and propulsion efficiency were given based on the resistive force theory. Section **4** analyzes the effects of geometrical parameters, including wire radius, helix pitch and helix length, on the swimming speed and efficiency. The optimal design of the swimmer to achieve a maximum speed at some constraints is also executed. Section **5** presents the experimental system for the helical swimmer actuation. Characterization of the microswmimmer is shown by experiments and compared with the theoretical results. Conclusion remarks are given in section **6**.

2 Structure of the artificial helical swimmer at submillimeter-scale

The basic structure of the single-end helical microswimmer is shown in Fig. 1a. A cylindrical magnet that is radically magnetized is adopted as the swimmer head for its easy fabrication. A helical structure is fixed on the end surface of the magnet. When a rotational magnetic field is generated in the plane normal to the axis of the cylinder, it rotates due to the applied magnetic torque. As a result, the spiral wave propagates and the swimmer propels itself. The helical microswimmers have been widely investigated in the last few years for their better swimming performances than gradient-pulling robots as their sizes decrease[16].

2.1.3 Experiment procedures

Motivated by the amphitrichous bacteria, a Double-End Helical Swimmer (DEHS) is proposed here, as shown in Fig. 1b. Comparing to the single-end helical swimmer, the double-end one has two helixes arranged at the two sides of the magnetic head. This structure is supposed to be advantageous due to the symmetry of the swimmer structure, and hence helpful to improve the forward-backward swimming symmetry.

(a) Single-end helical swimmer

(b) Double-end helical swimmer

Fig. 1 Helical swimmer structures.

3 Modeling the artificial helical swimmers

Firstly, the model of a single-end helical microswimmer is considered. Parameters of the swimmer are shown in Fig. 2. The Reynolds number is defined as the ratio of inertial force to viscous force, thus it quantifies the relative importance of the two types of forces for given flow conditions. The Reynolds number can be written as:

$$Re=\frac{\rho v d}{\eta}, \tag{1}$$

where ρ is the fluid density, v is the flow velocity, η is the fluid viscosity, d is the characteristic size of the object.

For submillimeter-scale swimmer, the Reynolds number in viscous fluid is much less than 1. In this case, the Navier-Stokes equation turns into the Stokes equation:

$$\nabla p+\eta\nabla^2 v=0, \tag{2}$$

where $p(r, t)$ is the pressure field.

3.1 Swimming velocity of the artificial helical microswimmer

For steady-state motion of the microswimmer, the drag on the swimmer balances the externally applied force and torque. A symmetric matrix was adopted to describe the helical movement by Purcell[19]:

$$\begin{bmatrix} f \\ \tau \end{bmatrix}=\begin{bmatrix} a & b \\ b & c \end{bmatrix}\begin{bmatrix} v \\ \omega \end{bmatrix}, \tag{3}$$

where f is the applied non-fluidic force, τ is the applied non-fluidic torque, v is the propulsion velocity, and ω is the rotational angular velocity. The coefficients in the propulsion matrix can be got by the resistive force theory[16]:

$$a=2\pi n\sigma\left(\frac{C_{\parallel}\cos^2\theta+C_{\perp}\sin^2\theta}{\sin\theta}\right), \tag{4}$$

$$b=2\pi n\sigma^2(C_{\parallel}-C_{\perp})\cos\theta, \tag{5}$$

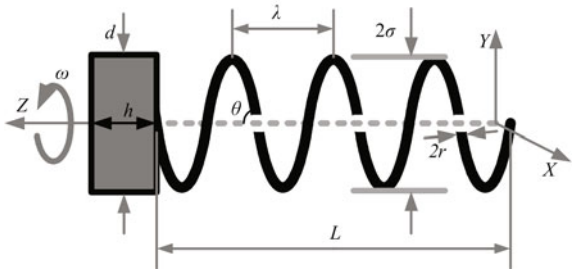

Fig. 2 Parameters of the helical swimmer.

$$c = 2\pi n\sigma^3\left(\frac{C_{\parallel}\sin^2\theta + C_{\perp}\cos^2\theta}{\sin\theta}\right), \tag{6}$$

where n is the turns number of the helix, σ is the helix diameter, θ is the pitch angle of the helix. $C_{\parallel}$ and $C_{\perp}$ denote the viscous coefficient parallel and normal to the cylindrical axis respectively. Lighthill proposed the following resistive coefficients[20]:

$$C_{\perp} = \frac{4\pi\eta}{\ln\frac{0.36\pi\sigma}{r\sin\theta} + 0.5}, \tag{7}$$

$$C_{\parallel} = \frac{2\pi\eta}{\ln\frac{0.36\pi\sigma}{r\sin\theta}}. \tag{8}$$

Gray and Hancock proposed the following coefficients [21]:

$$C_{\perp} = \frac{4\pi\eta}{\ln\frac{2\lambda}{r} + 0.5}, \tag{9}$$

$$C_{\parallel} = \frac{2\pi\eta}{\ln\frac{2\lambda}{r} - 0.5}, \tag{10}$$

where λ is the pitch of the helix, r is the radius of the helix wire. When the magnetic head is included, the propulsion matrix can be written as:

$$\begin{bmatrix} f \\ \tau \end{bmatrix} = \begin{bmatrix} a+\psi_v & b \\ b & c+\psi_\omega \end{bmatrix}\begin{bmatrix} v \\ \omega \end{bmatrix}, \tag{11}$$

where ψ_v and ψ_ω denote the resistive coefficient for the head in the translational and rotational directions respectively. The above equation can also be written as:

$$\begin{bmatrix} v \\ \omega \end{bmatrix} = \begin{bmatrix} \alpha & \beta \\ -\beta & \gamma \end{bmatrix}\begin{bmatrix} f \\ \tau \end{bmatrix}, \tag{12}$$

where

$$\alpha = \frac{1}{a+\psi_v}, \tag{13}$$

$$\beta = \frac{-b}{a+\psi_v}, \tag{14}$$

$$\gamma = c + \psi_\omega - \frac{b^2}{a+\psi_v}. \tag{15}$$

3.2 Propulsive force and efficiency of the artificial swimmer

As shown in Fig. 3, when a magnetic field with frequency ω is applied on the magnetized head of the microswimmer, the linear velocity of each element on the tail is $V_\theta=\omega\sigma$, thus the normal and tangential velocity is $V_n=V_\theta\cos\theta$ and $V_s=V_\theta\sin\theta$ respectively.

According to the resistive force theory, the normal and tangential components of drag force dF_n and dF_s on each element ds is:

$$dF_n = -C_{\perp}V_n ds, dF_s = -C_{\parallel}V_s ds, \tag{16}$$

In the Z direction, the propulsive force can be expressed as:

$$dF_z = dF_s\cos\theta - dF_n\sin\theta, \tag{17}$$

The total propulsive force F_z can be got by integration:

$$F_z = \int_0^{n\lambda} dF_z = n\lambda w\sigma\sin\theta(C_{\perp} - C_{\parallel}), \tag{18}$$

The torque element along the Z axis is:

$$dM_z = -\sigma(dF_s\sin\theta - dF_n\cos\theta). \tag{19}$$

The total generated torque M_z can be got by integration:

$$\begin{aligned} M_z &= \int_0^{n\lambda} dM_z \\ &= n\lambda w\sigma^2(C_{\perp}\cos^2\theta + C_{\parallel}\sin^2\theta)/\cos\theta, \end{aligned} \tag{20}$$

The propulsion efficiency η can be expressed as:

$$\eta = \frac{F_z v}{M_z\omega}. \tag{21}$$

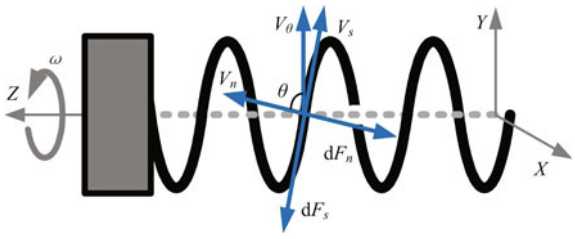

Fig. 3 Forces acting the helical swimmer.

3.3 The double-end helical microswimmer case

For the low Reynolds number condition, the propulsion matrix is linear[22]. Thus the double-end helical microswimmer with axial helix length of L_1 and L_2 at two ends can be treated as a single-end helical swimmer with tail length of L_1+ L_2. Accordingly, the model of single-end helical swimmer is also suitable for the double-end one.

4 Analysis and design of the helical microswimmer

The propulsion velocity and efficiency of the microswimmer have been got in Eqs. (12) and (21). For the analysis and design of a helical swimmer at submillimeter scale, a group of typical geometrical parameters of the swimmer were selected firstly. The parameters were selected mainly according to the latter experimental parameters. The diameter of the magnetic head is d= 0.8 mm, the height of it is h=0.4 mm. The helix radius σ is selected as 0.4 mm for convenient adhering with the magnetic head. The pitch λ=3 mm, the total helix length L=5 mm, the wire radius r=0.075 mm. The liquid viscosity is η=1000 mPa·s. The rotational angle velocity of the magnetic field is ω=20π rad·s^{-1}. The meanings of these parameters are shown in Fig. 2.

Fig. 4 shows effects of the wire radius on the velocity and propulsion efficiency of the microswimmer while keeping other parameters invariable. From the figure, the velocity and efficiency decrease with the increase of the wire radius. Thus it is preferable to choose a small wire radius to get a high propulsion speed or efficiency. However, considering the stiffness of the helix tail, the wire radius should not be too small.

Fig. 5 shows effects of the helix pitch on the propulsion velocity and efficiency of the microswimmer. From the figure, a peak value in the propulsion velocity occurs at about λ=2.7 mm. The velocity increases with the increasing pitch at first, then it decreases gradually with the increasing pitch after achieving a maximum velocity. The propulsion efficiency has a similar changing trend with the velocity, but the maximum efficiency occurs at about λ=2.5 mm.

Fig. 6 shows effects of the helix length on the velocity and propulsion efficiency of the microswimmer. From the figure, the velocity and efficiency increase with the increasing helix length. This indicates that a longer helix is advantageous to achieve a high propulsion velocity and efficiency.

Figs. 4–6 are based on the Lighthill's resistive coefficients, and similar results can be got by the coefficients of Gray and Hancock. From the above analysis, to achieve a high velocity and efficiency for the specific configuration, the wire diameter should be as small as possible while keeping the helix rigid, the pitch should be at 2.7 mm, and the tail length should be as large as possible when a geometrical constraint is satisfied.

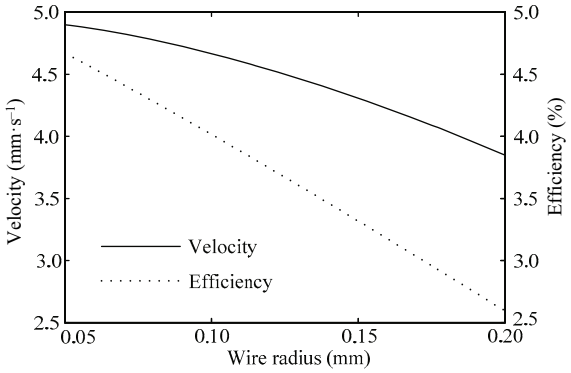

Fig. 4 Effects of the wire radius.

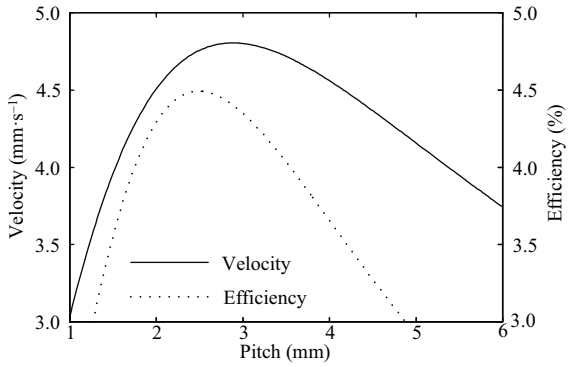

Fig. 5 Effects of the helix pitch.

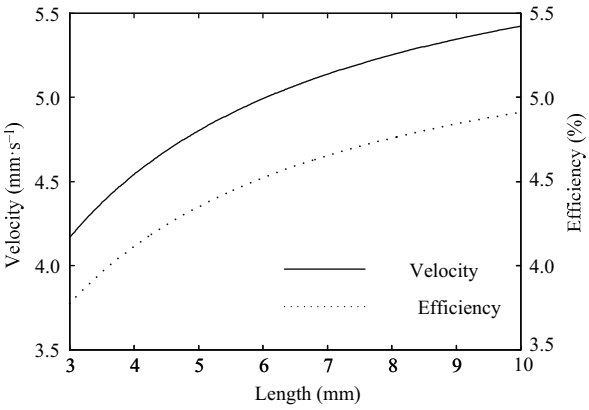

Fig. 6 Effects of the helix length.

5 Experiments

5.1 Experimental system

The experimental system of helical swimmers is shown in Fig. 7. It consists of three pairs of Helmoholtz coils which are placed orthogonally along the *X*, *Y* and *Z* axes. The Helmoholtz coils are driven by three Maxon servo controllers. The controllers are connected to a computer with a NI PCI-6733 analog output device. Two digital microscopes were used to observe the motion the swimmer from the top and side directions with recording rates of 100 frames per second.

To achieve a rotating magnetic field along an arbitrary axis, alternating currents are applied on each group of coils. For example, to get a rotating magnetic field B_0 along the *X* axis, the magnetic field B_y along the *Y* axis and B_z along the *Z* axis need to be controlled:

$$\begin{cases} B_y = B_0 \cos(2\pi ft) \\ B_z = B_0 \sin(2\pi ft + i\pi) \end{cases}, \quad (22)$$

where f is the rotational frequency. i=0, 1 control the magnetic field rotating along $+X$ or $-X$ direction.

5.2 Swimming performances of the single-end helical swimmer

A cylindrical magnet (NdFeB, diameter 0.8 mm, height 0.4 mm) magnetized in radial direction was selected as the swimmer head. For the helix tail, the diameter of the tungsten wire was 0.075 mm. The helix was formed by winding the tungsten wire on a winding machine. The magnetic head and the helix tail were adhered by the UV-curable adhesive.

For the helical microswimmer, the velocity is influenced by the helix pitch. Five groups of microswimmers were fabricated. They have the same magnetic heads, the same helix length L=5 mm. The swimmer velocities were measured at 10 Hz. Fig. 8 shows the effect of helical pitch on the swimming velocity. It can be seen that the maximum velocity is achieved when the pitch is 2.7 mm. From the figure, the experimental results are almost agree with the theoretical one, which indicates that there is an optimal value of the helix pitch to make the microswimmer get a maximum velocity.

Fig. 9 shows the effect of helical length on the swimming velocity. It can be seen that the velocity increases with the increasing helical length. From the figure, the real velocities are somewhat smaller than the theoretical ones. Besides the fabrication error, the resist theory may produce some error. According to the analysis in Ref. [23], when the ratio of the helix pitch to the helix radius is smaller than 8, the fluid interaction between each pitch can not be completely neglected, and the resistive force theory will bring some error. In this group of experiments, the ratio of the pitch to the radius of the microswimmer helix is about 6, so that some error may occur when the resistive force theory is adopted.

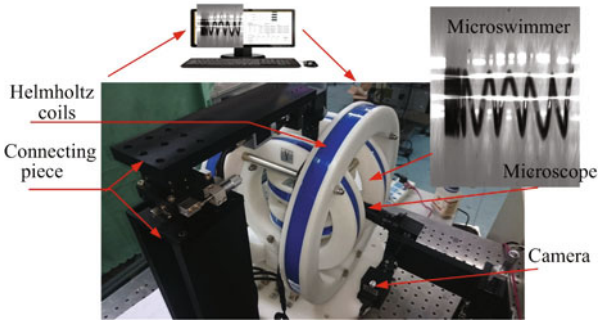

Fig. 7 Experimental system.

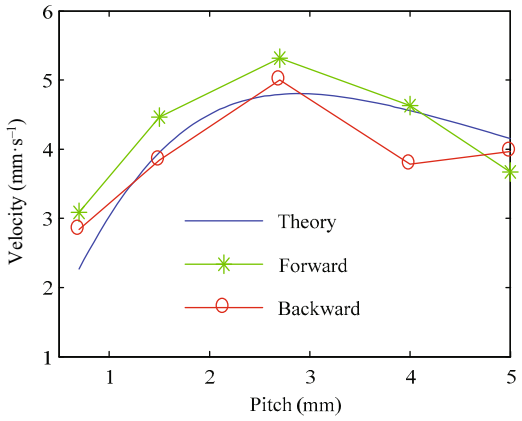

Fig. 8 Measured velocities for different helix pitches.

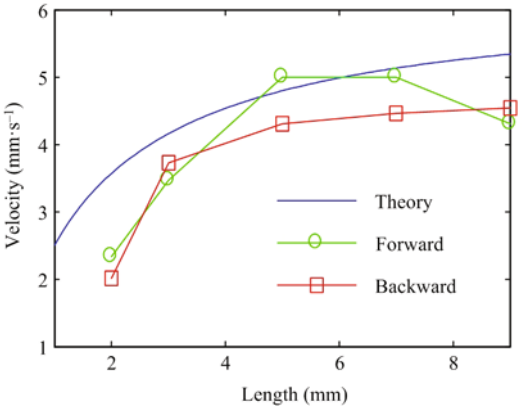

Fig. 9 Measured velocities for different helix lengths.

5.3 Swimming performances of the double-end helical swimmer

To compare the performance of the double-end helical swimmer to that of the sing-end one, the helix length of the former is made equal to that of the latter. The pictures of them are shown in Fig. 10. Here the helix length L=5 mm, the helix pitch λ=0.7 mm, the wire radius r=0.075 mm, the magnetic head is the same as the single-end helical swimmer in section **5.2**.

The performance of the double-end helical swimmer is shown in Fig. 11. From the figure, the velocity of the double-end swimmer approximately equals to the velocity of the single-end one, which indicates that the double-end swimmer can be thought as a superimposition of two single-end helical swimmers. To characterize the deviation of the forward velocity and backward velocity, the following deviation rate ε is defined as:

$$\varepsilon = \left| \frac{v_f - v_b}{v_f + v_b} \right| \times 100\%, \tag{23}$$

where v_f and v_b denote the forward and backward velocity respectively.

The deviations of the double-end helical swimmer and the single-end one are shown in Fig. 12. From the figure, the double-end helical swimmer has a smaller deviation comparing to the single-end one at high- frequency magnetic field. This is attributed to its symmetric geometric structure. When the frequency is smaller than 15 Hz, there are some velocity deviations for both swimmers, which is probably from the fabrication process. The forward-backward swimming asymmetry of single-end helical robots was also reported in Ref. [24]. For in vivo operations inside vessels, the precise motion control of the robot is highly desired and challenging. When the robot moves in the tiny tube, there is possibly no enough space for the swimmer to change directions abruptly, therefore the backward motion of the robot is necessary. At this case, the double-end helical swimmer is supposed to be advantageous for its easy control due to its forward-backward motion symmetry.

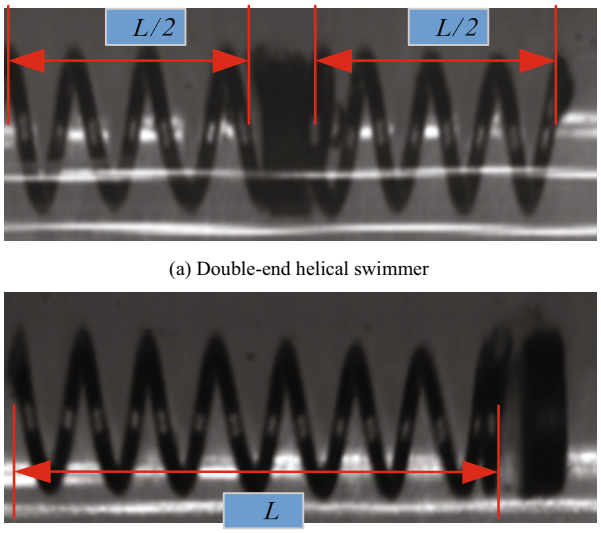

(a) Double-end helical swimmer

(b) Single-end helical swimmer

Fig. 10 Double-end and single-end helical swimmer.

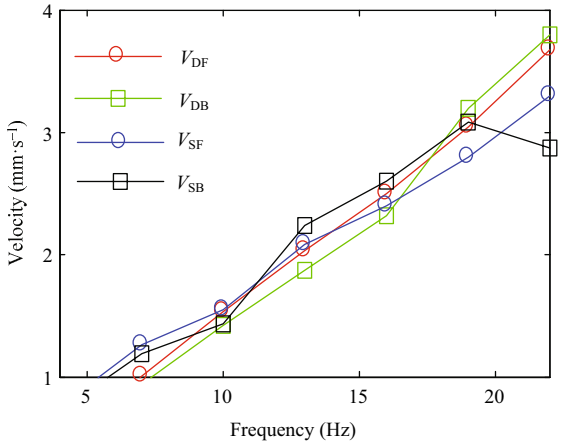

Fig. 11 Performance comparison of double-end helical swimmer and single-end one. V_{DF}, V_{DB} denote the forward and backward velocity of the double-end helical swimmer respectively. V_{SF}, V_{SB} denote the forward and backward velocity of the single-end helical swimmer respectively.

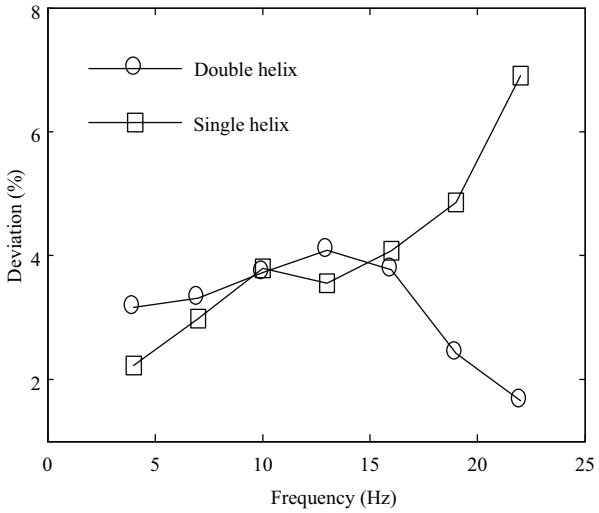

Fig. 12 Velocity deviation of the double-end helical swimmer and single-end one.

6 Conclusion

In this paper, the optimal design and motion characteristics of helical swimmers at submillimeter scale were investigated. Based on the conventional single-end helical swimmer, a double-end helical swimmer was proposed to improve the symmetry of the swimmer structure. The propulsion model of the artificial swimmer was described based on the resistive force theory. Influences of helix parameters on the swimming speed and propulsion efficiency were further analyzed. Then the optimal design for achieving a maximum speed was performed based on some constraints. An experimental system was built to control the motion of the helical swimmers. For single-end helical swimmer with different helix pitches, the effect curve of the pitch on the velocity has a maximum value. For single-end helical swimmer with different helix lengths, the effect trend of the length on the velocity was almost agree with the theoretical result. The measurement results of the double-end helical swimmer indicate that the superimposition of the helix length is suitable to model it. The velocity measurements also show that the double-end helical swimmer has better forward-backward motion agreement comparing to the single-end one. These results are helpful to design helical microswimmer for biomedical or micromanipulation applications. In the near future, the results will be verified on smaller helical microswimmers.

Acknowledgment

This work was supported by the Foundation for Innovative Research Groups of National Natural Science Foundation of China (No. 51521003), the Self-Planned Task of State Key Laboratory of Robotics and System (SKLRS201501A04), and the Scientific Research Foundation for the Returned Overseas Chinese Scholars, State Education Ministry.

References

[1] Nelson B J, Kaliakatsos I K, Abbott J J. Microrobots for minimally invasive medicine. *Annual Review of Biomedical Engineering*, 2010, **12**, 55–85.

[2] Chen B, Jiang S, Liu Y, Yang P, Chen S. Research on the kinematic properties of a sperm-like swimming micro robot. *Journal of Bionic Engineering*, 2010, **7**, S123–S129.

[3] Ha N S, Goo N S. Propulsion modeling and analysis of a biomimetic swimmer. *Journal of Bionic Engineering*, 2010, **7**, 259–266.

[4] Sitti M, Ceylan H, Hu, W, Giltinan J, Turan M, Yim S, Diller E. Biomedical applications of untethered mobile milli/microrobots. *Proceedings of the IEEE*, 2015, **103**, 205–224.

[5] Peyer K E, Tottori S, Qiu F, Zhang L, Nelson B J. Magnetic helical micromachines. *Chemistry-A European Journal*, 2013, **19**, 28–38.

[6] Ahmed D, Baasch T, Jang B, Pane S, Dual J, Nelson B J. Artificial swimmers propelled by acoustically activated flagella. *Nano Letters*, 2016, **16**, 4968–4974.

[7] He B, Wang Z, Liu C, Li Y, Shen R. Swimming behavior analysis based on bacterial chemotaxis in solution. *Journal of Bionic Engineering*, 2012, **9**, 315–321.

[8] Yang C, Chen C, Ma Q, Wu L, Song T. Dynamic model and motion mechanism of magnetotactic bacteria with two lateral flagellar bundles. *Journal of Bionic Engineering*, 2012, **9**, 200–210.

[9] Nain S, Sharma N N. Propulsion of an artificial nanoswimmer: A comprehensive review. *Frontiers in Life Science*, 2015, **8**, 2–17.

[10] Rao K J, Li F, Meng L, Zheng H, Cai F, Wang W. A force to be reck-oned with: A review of synthetic microswimmers powered by ultrasound. *Small*, 2015, **11**, 2836–2846.

[11] Belharet K, Folio D, Ferreira A. Three-dimensional controlled motion of a microrobot using magnetic gradients. *Advanced Robotics*, 2011, **25**, 1069–1083.

[12] Ishiyama K, Sendoh M, Yamazaki A, Arai K I. Swimming micro-machine driven by magnetic torque. *Sensors and Actuators A*, 2001, **91**, 141–144.

[13] Gao W, Feng X, Pei A, Kane C R, Tam R, Hennessy C, Wang J. Bioinspired helical microswimmers based on vascular plants. *Nano Letters*, 2014, **14**, 305–310.

[14] Ye Z, Régnier S, Sitti M. Rotating magnetic miniature swimming robots with multiple flexible flagella. *IEEE Transactions on Robotics*, 2014, **30**, 3–13.

[15] Yu T S, Lauga E, Hosoi A E. Experimental investigations of elastic tail propulsion at low Reynolds number. *Physics of Fluids*, 2006, **18**, 091701.

[16] Abbott J J, Peyer K E, Lagomarsino M C, Zhang L, Dong L X, Kaliakat-sos I K, Nelson B J. How should microrobots swim? *The International Journal of Robotics Research*, 2009, **28**, 1434–1447.

[17] Zhang L, Abbott J J, Dong L X, Kratochvil B E, Bell D, Nelson B J. Artificial bacterial flagella: Fabrication and magnetic control. *Applied Physics Letters*, 2009, **94**, 064107.

[18] Xu T T, Hwang G, Andreff N, Régnier S. Modeling and swimming property characterizations of scaled-up helical microswimmers. *IEEE/ASME Transactions on Mechatronics*, 2014, **19**, 1069–1079.

[19] Purcell E M. Life at low Reynolds number. *American Journal of Physics*, 1977, **45**, 3–11.

[20] Lighthill J. Flagellar hydrodynamics. *SIAM Review*, 1976, **18**, 161–230.

[21] Gray J, Hancock G J. The propulsion of sea-urchin spermatozoa. *Journal of Experimental Biology*, 1955, **32**, 802–814.

[22] Purcell E M. The efficiency of propulsion by a rotating flagellum. *Proceedings of the National Academy of Sciences of the United States of America*, 1997, **94**, 11307–11311.

[23] Rodenborn B, Chen C H, Swinney H L, Liu B, Zhang H P. Propulsion of microorganisms by a helical flagellum. *Proceedings of the National Academy of Sciences of the United States of America*, 2013, **110**, E338–E347.

[24] Temel F Z, Yesilyurt S. Confined swimming of bio-inspired microrobots in rectangular channels. *Bioinspiration & Biomimetics*, 2015, **10**, 016015.